applied sciences

MDPI

Article

Research of Enzyme-Induced Carbonate Precipitation on Strength Behavior of Reinforced Sand

Jianye Wang [1], Xiao Li [1], Liyun Peng [1,*], Shuang Lu [1], Jin Zhang [1] and Xintao Du [2]

[1] School of Civil Engineering and Transportation, Beijing University of Civil Engineering and Architecture, Beijing 100044, China; wangjianye@bucea.edu.cn (J.W.); 19801305720@163.com (X.L.); 2108590124014@stu.bucea.edu.cn (S.L.); zj18152160456@163.com (J.Z.)
[2] Beijing Institute of Engineering Geology, Beijing 100037, China; dxt13934310093@163.com
* Correspondence: pengliyun@bucea.edu.cn; Tel.: +86-13901329162

Abstract: Stabilizing sandy soil with inadequate engineering properties is essential for constructing infrastructure systems in all regions, especially in desertification-prone areas. Enzymatically Induced Carbonate Precipitation (EICP) offers an innovative solution, with advantages over conventional soil reinforcement methods due to its low energy consumption and carbon emission. This emerging reinforcement technique has proven effective in enhancing soil strength, yet the effects of variables such as curing time and cementation solution concentration, and their micro-mechanistic implications on sandy soil, remain understudied. This study conducted a series of unconfined compressive strength (UCS) tests and microstructural analyses on EICP-treated sand. The results showed that the optimal curing time for EICP-reinforced sand is seven days, with its strength being contingent upon soil density. The maximum UCS value was observed at a relative density of 0.7 and a cementation solution concentration of 1 mol/L. Mechanistically, EICP strengthens soil integrity through calcium carbonate-mediated cementation and particle bridging, thereby boosting soil strength. Micro-CT imaging and fractal dimension analyses reveal that the precipitation process decreases both the size and connectivity of the pores, while simultaneously increasing their surface heterogeneity and enhancing the overall toughness. This research establishes a foundational framework for advancing EICP applications in soil stabilization engineering.

Keywords: Enzymatically Induced Carbonate Precipitation (EICP); soil strength improvement; micro-CT; fractal dimension; pore structure

check for updates

Academic Editor: Tiago Filipe da Silva Miranda

Received: 22 February 2025
Revised: 15 March 2025
Accepted: 17 March 2025
Published: 25 March 2025

Citation: Wang, J.; Li, X.; Peng, L.; Lu, S.; Zhang, J.; Du, X. Research of Enzyme-Induced Carbonate Precipitation on Strength Behavior of Reinforced Sand. *Appl. Sci.* **2025**, *15*, 3558. https://doi.org/10.3390/app15073558

Copyright: © 2025 by the authors. Licensee MDPI, Basel, Switzerland. This article is an open access article distributed under the terms and conditions of the Creative Commons Attribution (CC BY) license (https://creativecommons.org/licenses/by/4.0/).

1. Introduction

With rapid urbanization and infrastructure expansion globally, construction in geotechnically challenging environments—such as desertified regions requiring sand stabilization—has become imperative. Typically, the sandy soil prevalent in these areas requires reinforcing through methods like tamping [1,2] or chemical grouting [3,4] before being used as construction materials. However, these traditional soil stabilization techniques are associated with considerable energy consumption and a substantial carbon footprint during both material production and utilization phases, which may pose risks of environmental harm and ecosystem disruption [5,6]. Consequently, bio-cementation has emerged as a sustainable alternative, garnering attention for its eco-friendliness and high efficiency in calcium carbonate yield [7–11]. Among bio-cementation approaches, Microbially Induced Carbonate Precipitation (MICP) and Enzyme-Induced Carbonate Precipitation (EICP) are widely studied. MICP relies on bacteria (e.g., *Sporosarcina pasteurii*) to hydrolyze urea,

producing carbonate ions for $CaCO_3$ precipitation. In contrast, EICP directly utilizes plant-derived or commercial urease (Figure 1), eliminating bio-safety concerns associated with bacterial use. Moreover, urease's smaller molecular size enhances its mobility in soil pores, potentially improving treatment uniformity [12,13].

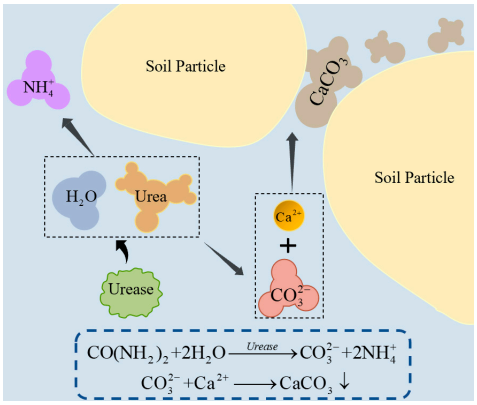


Figure 1. Mechanisms of the enzyme-induced calcite precipitation (EICP) technique.

Recent research has demonstrated that the Microbially Induced Carbonate Precipitation (MICP) significantly enhances the mechanical properties of sandy soils, including improving strength [14,15], reducing permeability by blocking pores [16,17], and mitigating wind erosion [18,19]. Conversely, the impact of the EICP technique on reinforcing sandy soils has received comparatively less attention. The available studies predominantly indicate that EICP effectively increases the strength of sandy soils [20–24]. However, the imperfections in the research still limit the application of this technology in geotechnical engineering. For instance, investigations into the micro-mechanisms of EICP-reinforced sand have primarily used scanning electron microscopy (SEM), which does not fully capture the three-dimensional effects of precipitate aggregation and distribution within the soil [21,25]. Furthermore, the complexity of pore structures can vary even with the same amount of EICP precipitation, affecting the soil's properties. However, quantitative descriptions of pore structure in EICP-reinforced soils and their relationships with soil strength (e.g., fractal dimension) are rare in the literature.

To address these gaps, this paper investigates the strength behavior and micro-mechanisms of sand reinforced by EICP, evaluating the effects of varying densities and cementation solution concentrations. The paper also provides a comparative analysis of the EICP reinforcement mechanism using SEM, three-dimensional micro-computed tomography (CT) scans, and fractal dimension analysis, aiming to clarify the strength response and underlying mechanisms of EICP-reinforced sandy soil for future engineering applications.

2. Materials and Methods

2.1. Materials

The soil used in the tests was Fujian standard sand (Xiamen, China), a commercially available material widely used in academic research and the construction industry across China. Figure 2 illustrates the particle size distribution curve and provides a visual representation of the soil. The basic physical indexes of the sand were determined following the standards outlined in [26]. The results shows that the specific gravity of the soil is 2.65, with maximum and minimum dry densities of 1.98 and 1.62, respectively. Based on the characteristics reflected by the experimental data, it can be inferred that this sand is a quartz sand with relatively smooth grains, and it exhibits significant differences in mechanical properties under different relative densities.

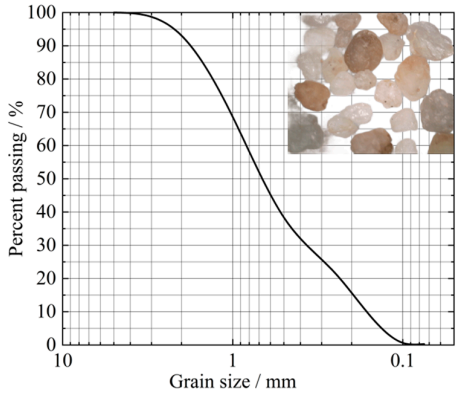


Figure 2. PSD curves and physical appearance (50×) of the sand used in the tests.

For the EICP process, the urease enzyme used was extracted from soybeans (Dalian, China), and the extraction process is detailed below (see Figure 3 for a visual representation of the procedure): The soybeans were dried and pulverized, after which the powder was sifted and mixed with deionized water in a solid-to-liquid mass ratio of 1:10. This mixture was then stirred and centrifuged. The supernatant was collected and filtered again. To measure the urease activity, the Nessler method as mentioned in Khodadadi [27] was employed. The measured urease activity in this study was 6.777 mM/L/min, and the value showed little variation when monitored over a period of 28 days.

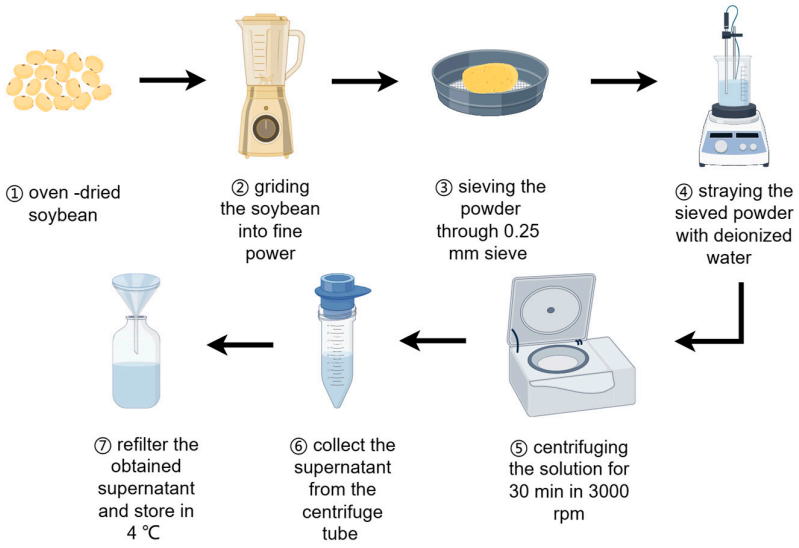


Figure 3. Extraction procedure of soybean urease in this study.

2.2. Methods

2.2.1. Sample Preparation

The soil sample for the unconfined compressive strength (UCS) test was cylindrical, measuring 39.1 mm in diameter and 80 mm in height. The specimens were compacted at different relative densities (D_r), which were controlled by the dry densities of the soil. The details of EICP sample preparation are described here:

1. EICP solution (equal volumes of urease solution and cementation solution) was mixed at 1.1 times the pore volume, as calculated based on the dry density of the soil [28], with sand.
2. This mixture was then compacted into the mold in three layers to ensure uniformity.
3. The compacted samples were subsequently cured at a constant temperature of 25 °C and a relative humidity of 50% for a predetermined curing period.

4. Finally, the samples were demolded and oven-dried to constant weight.

2.2.2. Test Procedure

The unconfined compressive strength (UCS) tests were produced in two groups, at a displacement rate of 0.5 mm/min. Samples with varying curing times d (1, 3, 5, 7, and 28 days) and relative densities (D_r = 0.6, 0.7, 0.8, 0.9) were tested at a cementation solution concentration of C = 1.0 mol/L to identify the optimal curing time [22,29]. In the second group, samples with different D_r and C values were tested using the previously determined optimal curing time. SEM tests were performed on this group of soil samples. Also, calcium carbonate precipitation (W) was quantified via the acid-wash method [14]. Micro-CT analysis was conducted on samples with D_r = 0.7 to assess 3D pore distribution, with a plain soil specimen (C = 0) as a control. For micro-CT, a 10 mm cube segment was scanned at 120 kV, 150 μA, and 7 μm resolution, producing 500 slice images. Raw CT images were processed and reconstructed using Avizo software (Version 2020.1). Details of the test plan are summarized in Table 1.

Table 1. Test program of this study.

Test	Curing Time d Day	Relative Densities D_r	Cementation C mol/L
UCS-1	1, 3, 5, 7, 28	0.6, 0.7, 0.8, 0.9	1.0
UCS-2	Optimal curing time	0.6, 0.7, 0.8, 0.9	0.5, 1.0, 1.5, 2.0
SEM	Optimal curing time	0.6, 0.7, 0.8, 0.9	0.5, 1.0, 1.5, 2.0
$CaCO_3$ quantify	Optimal curing time	0.6, 0.7, 0.8, 0.9	0.5, 1.0, 1.5, 2.0
Micro-CT	Optimal curing time	0.7	0, 0.5, 1.0, 1.5, 2.0

3. Results and Discussion

3.1. Unconfined Compressive Strength

3.1.1. Influence of Curing Time on Strength

The variation in UCS of EICP-reinforced sand samples with different densities and curing times is depicted in Figure 4.

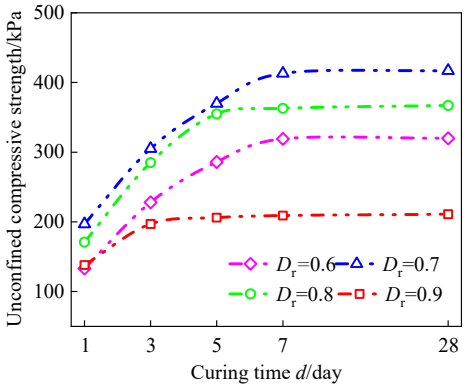


Figure 4. Variation in UCS of EICP-reinforced sand with curing time.

It can be seen that the strength of soil samples generally increased with curing time, peaking within the tested duration. Notably, the strength of EICP-reinforced soil samples at all densities exhibited a significant increase as the curing time extended from 1 to 3 days, due to the incomplete reaction of the cementing solution and limited calcium carbonate formation initially. After 3 days, the strength increase was marginal for the sample with D_r = 0.9, as higher density reduced pore volume, and the calcium carbonate formed initially was less effective in filling smaller pores. For samples with D_r = 0.8, the reaction took

5 days to complete, after which no significant strength increase occurred. For samples with lower densities (D_r = 0.7 and D_r = 0.6), the strength peaked at 7 days, due to larger pores accommodating more calcium carbonate. Beyond 7 days, strength did not increase significantly, indicating the reaction was near completion. The ideal curing time was thus identified as 7 days, and future experiments used this duration. It was also observed that the optimum curing time decreased with higher D_r, suggesting a correlation between pore scale and calcium carbonate formation efficiency. Smaller pores may limit calcium carbonate precipitation, but further studies are needed.

3.1.2. Influence of Relative Density on Strength

Figure 5 demonstrates the variations in UCS of EICP-reinforced sand as influenced by relative density (D_r) and cementation solution concentration (C) after a curing time of 7 days. The results in Figure 5 show two distinct patterns in the strength of the samples as D_r increases, depending on the cementation solution concentration. At 0.5 mol/L, strength increases steadily with D_r. However, at higher concentrations (1.0~2.0 mol/L), strength initially rises with D_r, peaks at D_r = 0.7, and then sharply decreases. Due to the generally lower strength at 0.5 mol/L, the optimal relative density, D_r = 0.7, was selected for further analysis.

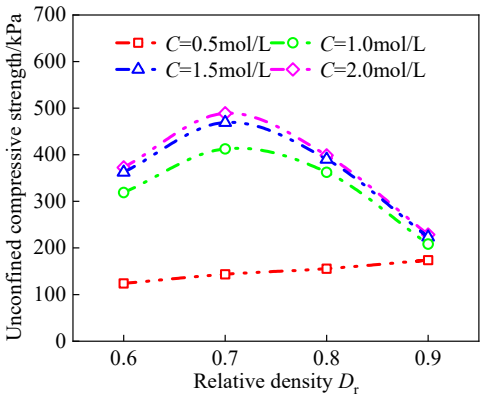


Figure 5. Variation in UCS of EICP-reinforced sand with relative density.

This behavior can be explained as follows: at 0.5 mol/L, the low concentration of urea and calcium ions limits the formation of calcium carbonate crystals, resulting in insufficient reinforcement and lower strength. In this case, soil friction, governed by the sand's void ratio, is the primary factor influencing strength, leading to a steady increase as D_r increases. In contrast, higher concentrations promote more calcium carbonate precipitation, enhancing cementation and surface friction between soil particles. As D_r increases, however, the reduced void space limits the EICP solution volume, decreasing $CaCO_3$ precipitation and lowering strength. Thus, the strength of EICP-reinforced sand is a combination of the plain soil strength and the reinforcement effect, with the optimal outcome occurring at D_r = 0.7, where both factors are balanced.

3.1.3. Influence of Cementation Solution Concentration on Strength

Figure 6 displays the variations in UCS of EICP-reinforced sand as influenced by cementation solution concentration (C) after a curing time of 7 days. It can be seen that the UCS of EICP-reinforced sand increases with cementation solution concentration (C) at different D_r values. At 0.5 mol/L, strength remains low and positively correlates with D_r. Significant strength improvement occurs when the concentration increases from 0.5 mol/L to 1 mol/L, with strength enhancements exceeding 200% for D_r values of 0.6, 0.7, and 0.8. However, no significant increase is observed at concentrations above 1 mol/L, indicating

that the reinforcement effect is limited beyond this threshold, likely due to urease catalysis inhibition. Consequently, it can be concluded that the optimal C value for this study is 1 mol/L. Under this concentration, the soil sample with D_r = 0.7 exhibits the maximum UCS value of 413 kPa.

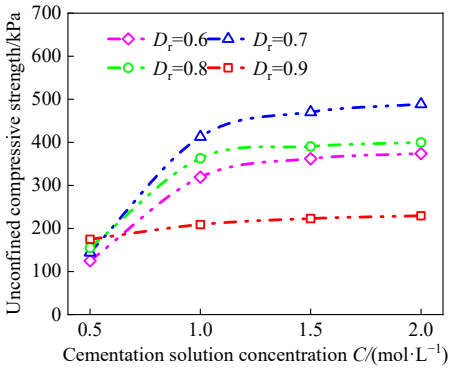


Figure 6. Variation in UCS of EICP-reinforced sand with cementation solution concentration.

3.1.4. Correlation Analysis Between Variables and Strength

To quantitatively investigate the correlation between D_r, C, d, and UCS, a linear correlation analysis was conducted using Pearson's correlation coefficient [30], as shown in Equation (1).

$$R(x,y) = \frac{\sum_{i=1}^{n} x_i y_i - n\overline{x}\,\overline{y}}{\sqrt{\sum_{i=1}^{n}\left(x_i^2 - n\overline{x}^2\right)\sum_{i=1}^{n}\left(y_i^2 - n\overline{y}^2\right)}} \quad (1)$$

where x_i and y_i are the observed values of the i-th sample, $\overline{x}$ and $\overline{y}$ are the means of the variables x and y, and n is the sample size.

As shown in Figure 7, the Pearson correlation coefficients reveal the following relationships: D_r shows a weak negative correlation (−0.23) with UCS, suggesting that increased soil density slightly suppresses strength; C exhibits a moderate positive correlation (0.62), indicating that higher concentrations significantly enhance sandy soil strength; and d has a weak positive correlation (0.43), implying limited strength gain from extended curing beyond an initial period.

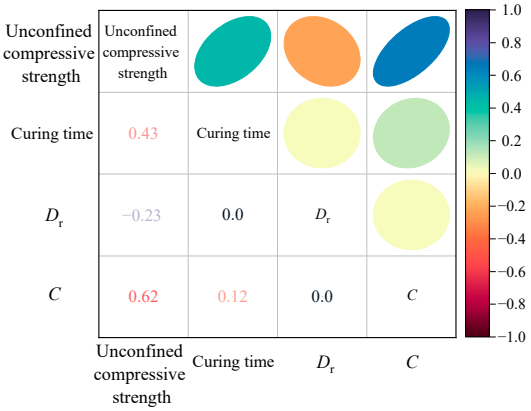


Figure 7. Heatmap of Pearson correlation coefficients in this study.

3.1.5. Relationship Between Calcium Carbonate Content and Strength

Figure 8 illustrates the variation in calcium carbonate content (W) of EICP-reinforced soil in relation to C across different D_r and how this relates to the corresponding UCS. It can be seen that for a given D_r, W increases up to 7% with increasing C, though this upward trend gradually slows. This is because a higher solution concentration provides

more reactants for the reaction, thereby producing more precipitate. Notably, at a *C* value of 1 mol/L and D_r = 0.7, the precipitation content peaks at 6%, coinciding with the maximum UCS value. This finding aligns with the results presented in Figure 6, suggesting a close correlation between the strength of EICP-reinforced soils and the quantity of calcium carbonate formed. Furthermore, for soil with the same *C*, the calcium carbonate content diminishes as D_r increases, a trend that supports the observations from Figure 5. Based on the discussion above, one can find that for soil samples with a certain D_r, soil strength is positively correlated to *W*. However, strength is not solely determined by *W* when D_r varies.

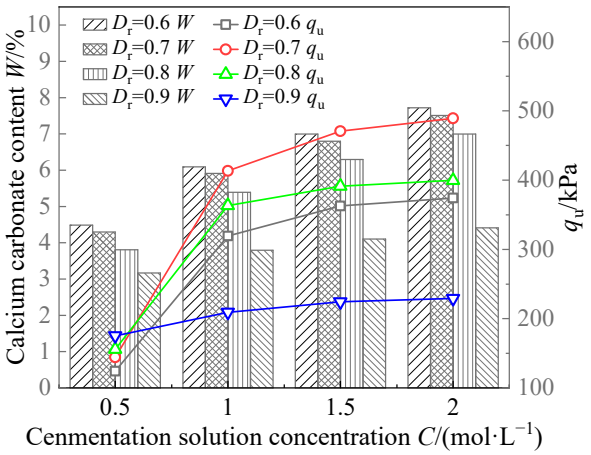


Figure 8. Relationships between *W* and UCS of different EICP-reinforced samples.

The relationship between calcium carbonate content and *C* shown in Figure 8 is non-linear, indicating that only a portion of Ca^{2+} participates in the reaction. To quantitatively describe the extent of the reaction, the average conversion rate of calcium ions (η) was calculated according to Equation (2).

$$\eta = \frac{n_{CaCO_3}}{\eta_0^{Ca^{2+}}} \times 100\% \quad (2)$$

where η_{CaCO_3} represents the molar amount of calcium carbonate produced and $\eta_0^{Ca^{2+}}$ represents the initial molar amount of Ca^{2+} in the cementation liquid.

As shown in the Figure 9, with the increase in *C* from 0.5 to 2 mol·L^{-1}, the conversion rate of calcium ions gradually decreased from 89.4% to 38.5%. This is because when the concentration of Ca^{2+} exceeds 1 mol·L^{-1}, Ca^{2+} competitively binds to the active sites of urease, reducing the efficiency of urea hydrolysis by urease and thereby inhibiting the formation of calcium carbonate crystals. This is consistent with previous studies [31] that reported the inhibitory effect of Ca^{2+} on urease activity.

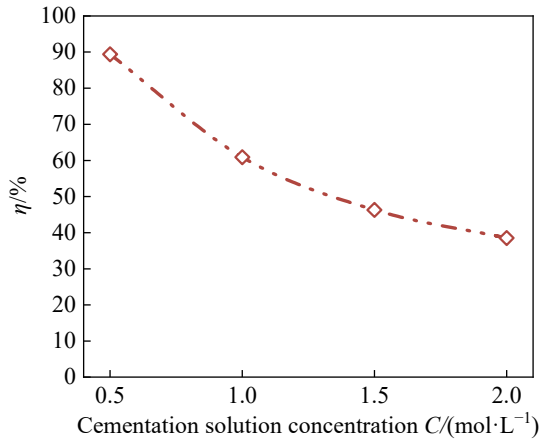


Figure 9. Relationships between *C* and conversion rate of calcium ions.

3.2. Micro-Mechanism of EICP-Reinforced Sand

3.2.1. Crystal–Soil Cementation Patterns

The crystal–soil cementation patterns refer to three distinct microstructural mechanisms (shown in Figure 10) through which enzymatically precipitated calcium carbonate ($CaCO_3$) interacts with sand particles to enhance mechanical strength. The spatial distribution characteristics and bonding morphology of crystals observed in SEM images can be systematically categorized as follows:

1. Bonding effect (red arrows): Calcium carbonate precipitates around points of contact between soil particles, effectively binding them together and enhancing their interaction. This effect is most noticeable in particles with plane–plane contacts, where the extended contact surface facilitates greater crystal aggregation, resulting in stronger cementation.
2. Bridging effect (blue arrows): When soil particles are not directly in contact, calcium carbonate crystals form on the particle surfaces and grow to bridge the intergranular pores. This "bridging effect" strengthens the overall soil structure by connecting the particles and improving its integrity.
3. Encapsulating effect (yellow arrows): Calcium carbonate crystals that form on isolated soil particles gradually accumulate and encapsulate the particles. While this does not directly enhance soil cohesion, it increases intergranular friction, especially in cases where particles are prone to rotation or sliding.

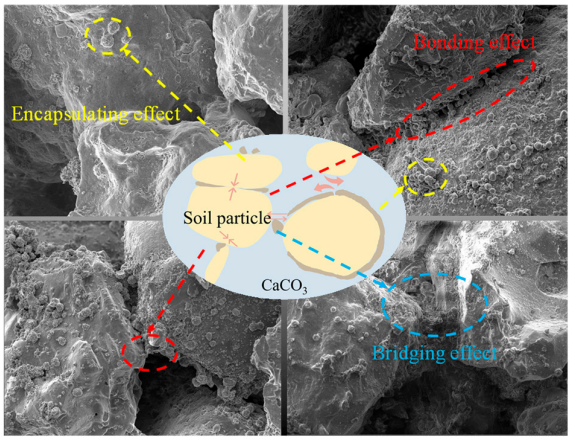


Figure 10. Different cementation patterns of EICP-reinforced sand.

These three cementation modes collectively form a hierarchical reinforcement system: The bonding effect establishes the primary framework (first level), the bridging effect forms

the secondary support (second level), and the encapsulating effect optimizes stress transfer efficiency through interfacial modification (third level).

3.2.2. Influence of EICP on Pore Distribution of Soil

The analysis of the influence of EICP on the pore structure of soil is based on image processing of CT scan results. As shown in Figure 11, slices obtained from the CT scans were 3D reconstructed using Avizo software (Version 2020.1) to generate the pore space distribution model. The pore distribution was then transformed into a Pore Network Model (PNM) by extracting the geometric characteristics of the pores. Connectivity analysis was employed to distinguish between isolated and connected pores. Both the pore space distribution model and the PNM were used to characterize various pore properties.

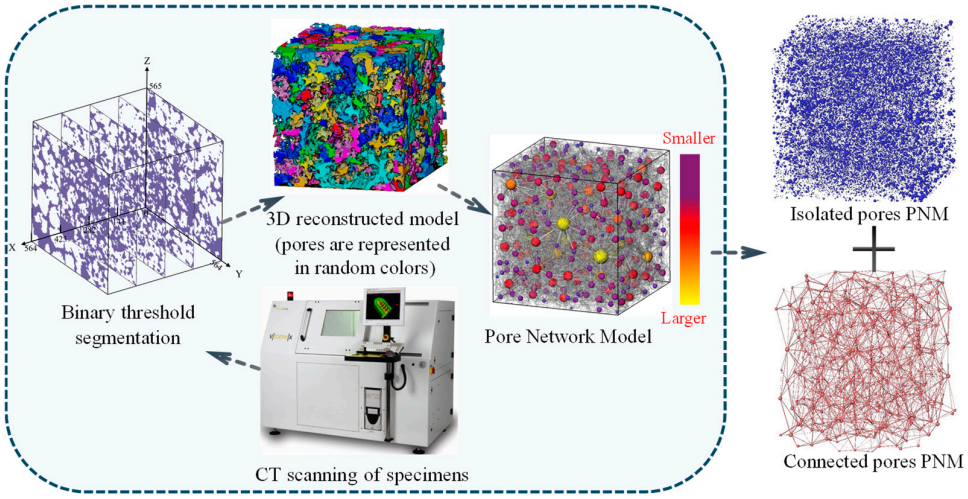


Figure 11. Steps for imaging processing of CT test results.

Table 2 presents the pore statistical information and pore volume distribution in plain soil (CT0) and EICP-reinforced samples with cementation solution concentrations of 0.5, 1, 1.5, and 2 mol/L (CT1, CT2, CT3, and CT4, respectively). For pore size distribution statistics, the pores are categorized by size into three groups: large (>1.4 × 10^8 μm^3), medium (4.4 × 10^7–1.4 × 10^8 μm^3), and small (<4.4 × 10^7 μm^3). Table 2 shows that as the cementation solution concentration increases from 0 mol/L to 2 mol/L, the porosity decreases significantly from 30.92% to 15.01%, a reduction of 51.5%. Furthermore, it is evident that both large and medium pores decrease noticeably, while small pores tend to increase. This phenomenon is specifically illustrated in the statistical data presented in Figure 12.

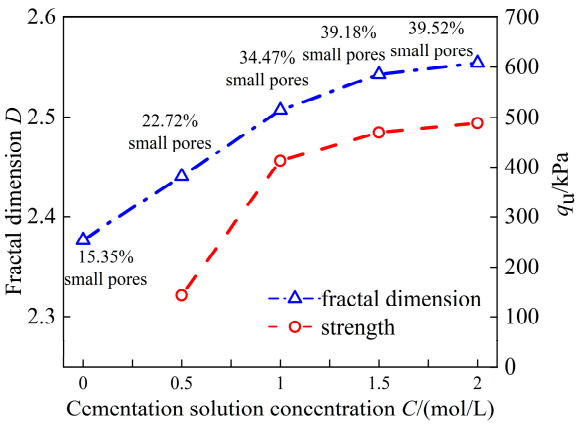
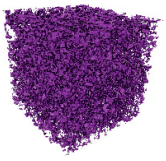
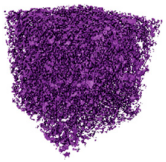
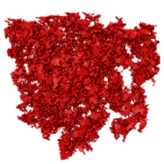
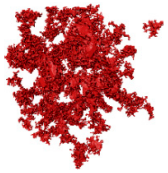
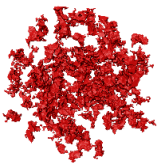
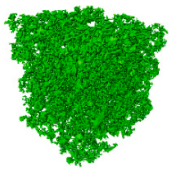
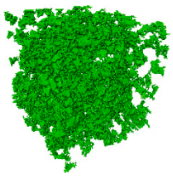
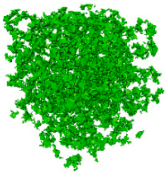
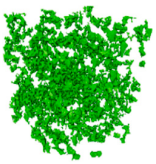
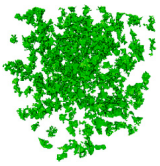
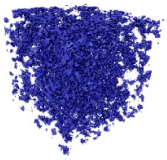
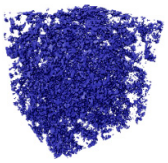
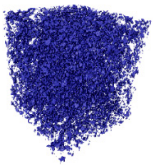
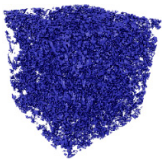
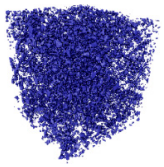
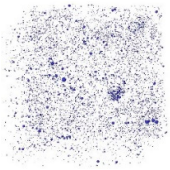
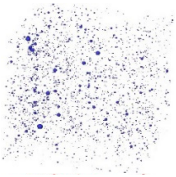
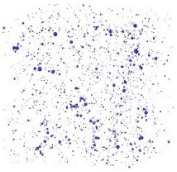
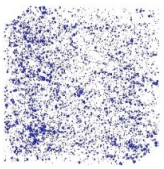
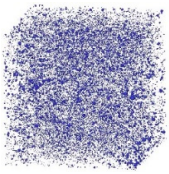
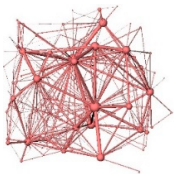
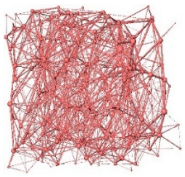
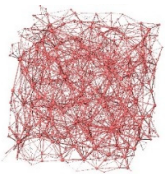
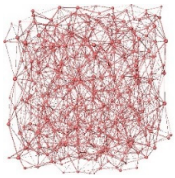
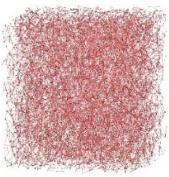


Figure 12. Variation in pore volume in EICP-reinforced sand at D_r = 0.7.

Table 2. Pores distribution and porosity statistics of different soil samples at D_r = 0.7.

Item	CT0	CT1	CT2	CT3	CT4
Porosity (%)	30.92	22.17	18.22	16.45	15.01
Integral pores					
Large pores					
Medium pores					
Small pores					
Isolated pores (%)	3.60	9.55	12.76	14.43	15.39
Isolated pores					
Connected pores					
Euler number	−88,143	−58,289	−51,665	−49,144	−47,592

The results in Figure 10 show a decrease in total pore volume as *C* increases. Specifically, both large and medium pores decrease in volume with higher *C*, while small pores initially increase from 0 (plain soil) to 1.5 mol/L. This is due to large and medium pores storing more solution, facilitating crystal aggregation around adjacent particles. As crystal size increases, it blocks pore throats, subdividing large or medium pores into smaller ones. The reduction in large pores indicates particle bonding and bridging effects. However, from *C* = 1.5 to 2 mol/L, small pores decrease in volume. This suggests that higher concentrations of the reaction solution promote more calcium carbonate precipitation, leading to the blocking of smaller pores.

3.2.3. Influence of EICP on Pore Connectivity of Soil

The connectivity of soil pores critically governs mechanical behavior, as interconnected pores tend to evolve into continuous microcracks under stress, ultimately leading to structural failure. The analysis reveals that EICP treatment systematically modifies pore

connectivity through the isolated pore ratio. In addition, the Euler number ($\chi = b_0 - b_1 + b_2$, where b_0 = individual pores, b_1 = pore throats, and b_2 = pore-surrounded solid clusters) can also be used to characterize pore connectivity; the higher the Euler number, the poorer the connectivity. The results from Table 2 show that as *C* increases, the number of isolated pores gradually increases, while the pore throat radius between the connected pores decreases. The evolution of connected pores can be divided into three stages: (1) Sensitive response period (0~1.0 mol/L): During this stage, large-scale pores are preferentially filled, leading to the fracture of the main connected channels, resulting in a significant increase in strength. (2) Reinforcement transition period (1.0~1.5 mol/L): Smaller secondary pores are sealed, and the strength increases modestly. (3) Stabilization period (1.5~2.0 mol/L): The pore network is further refined and the strength stabilizes.

Overall, the strength enhancement is closely related to the evolution of the pore structure, and conclusions about the connectivity of EICP-reinforced soil can be made as follows:

- Degradation of Connectivity: The proportion of connected pores decreases from 96.3% at 0 mol/L to 84.51% at 2 mol/L, while the proportion of isolated pores increases from 3.6% to 15.39%.
- Topological Discretization: The Euler number decreases from −88,143 at 0 mol/L to −47,592 at 2 mol/L, indicating that the pore network transitions from highly connected to isolated clusters.

3.2.4. Influence of EICP on Fractal Dimension of Soil

The fractal dimension reflects the complexity, shape intricacy, and surface roughness of the pore structure. Based on micro-CT scan results, the fractal dimension (*D*) of EICP-reinforced sand at different *C* was calculated using the box-counting method [32], as shown in Figure 13. The ratios of small pore volumes and the strength of different specimens are also presented. As *C* increases, the fractal dimension of the soil also increases, indicating that $CaCO_3$ precipitation contributes to greater pore surface roughness and more heterogeneous pore structures. The trends in the proportion of small pores and fractal dimension are similar, due to the larger specific surface area of small pores. The fractal dimension reflects the soil's microstructure, which plays a key role in its mechanical properties [33]. As shown in Figure 13, the changes at the microscale align with macroscopic observations: both strength and fractal dimension initially improve significantly (from 0.5 to 1.5 mol/L) and then stabilize (from 1.5 to 2 mol/L). This pattern suggests that the increase in fractal dimension—indicating more roughness and irregularity in pore surfaces—enhances interparticle friction, thereby strengthening the soil through both cohesion and friction.

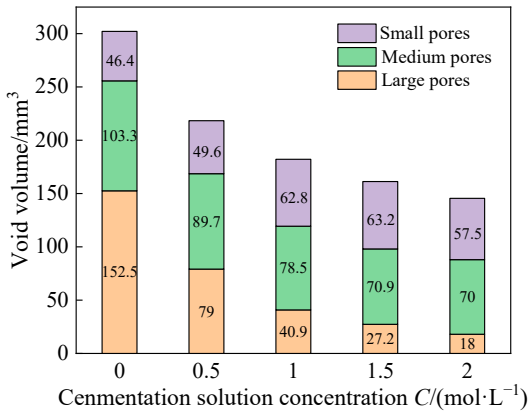


Figure 13. Variation in fractal dimension and strength of EICP-reinforced sand at D_r = 0.7.

3.2.5. Micro-Mechanism of EICP Reinforcement

Based on the UCS test results and the microscale analysis, the micro-mechanisms underlying the macro-phenomena of strength improvement by EICP can be outlined. Firstly, the morphology of the crystals influences their cementation patterns. Small, discrete crystals (Figure 10) are insufficient for bonding soil particles but tend to fill smaller pores, encapsulate particle surfaces, and bond particles at contact points. In contrast, larger, aggregated crystals can bond soil particles, fill larger voids, and bridge separated particles. Secondly, the calcium carbonate aggregates formed in the large pores of the soil can subdivide the large pores into several smaller ones and split the connected pores into isolated pores. This reduces the formation of fine fracture surfaces during the loading process, thereby increasing the overall strength of the soil. Finally, from a fractal dimension perspective, the improvement in sand strength through EICP is attributed to the increased irregularity and toughness of the pore structure, induced by calcium carbonate precipitation. This pattern, characterized by the fractal dimension, shows a positive correlation within the scope of this study.

4. Conclusions

Soil reinforcement has long been a critical area of study in civil engineering, particularly for improving the mechanical properties of sandy soils, which are often prone to instability. Enzyme-Induced Carbonate Precipitation (EICP) has emerged as a promising eco-friendly soil stabilization method. However, the mechanisms underlying the strength improvement of EICP-reinforced sand remain poorly understood. In this paper, EICP is hypothesized to enhance the strength of sandy soil by bonding soil particles. The strength behavior and micro-mechanism of EICP-reinforced sand were investigated through a series of UCS, SEM and Micro-CT tests. The following key conclusions can be drawn:

(1) As the curing time increases, the strength of EICP-reinforced sand progressively increases, reaching a maximum at 7 days. After this period, no significant increase in strength is observed, indicating a plateau effect. The strength is a composite outcome of the inherent strength of the plain soil and the reinforcement provided by EICP, which is strongly influenced by the relative density (D_r) of the unreinforced sand and cementation solution concentration (C). The maximum reinforcing effect occurs when D_r is 0.7 and C is 1 mol/L.

(2) At a microscale, strength improvement is attributed to the three tier modes resulting from precipitation, namely bonding, bridging, and encapsulating effects of the precipitation, which are influenced by specific crystal morphologies that enhance particle bonding.

(3) EICP precipitation contributes to the disintegration of large pores and reduces the total pore volume within the soil. When cementation solution concentration exceeds 1.5 mol/L, small pores tend to be occupied and blocked by the crystals exhibiting an encapsulating effect, which results in a slight increase in strength. This trend substantiates the essence of the strength improvement achieved by the EICP technique, which involved binding particles together and increasing inter-particle friction.

(4) As the cementation solution concentration increases, the proportion of connected pores decreases, and isolated pores become more prevalent. This degradation of pore connectivity hinders the formation of continuous microscopic failure surfaces, contributing to the observed strength enhancement.

(5) Fractal dimension analysis shows that as cementation solution concentration increases from 0 to 1.5 mol/L, pore toughness and heterogeneity rise from 2.38 to 2.54, showing an increase of nearly 7%, indicating the formation of aggregated particles and higher

inter-particle friction. This trend correlates with the observed increase in strength and offers further insight into the strengthening mechanisms.

According to the conclusions above, the research hypothesis was proven correct through experiments and analysis. As a novel soil reinforcement technique that is low-carbon and environmentally friendly, EICP has been proven to enhance the strength of sandy soil in a short period of time, which endows it with the potential for application in engineering projects such as foundation reinforcement and embankment construction. However, the current studies on EICP-reinforced sand are still in the laboratory stage and focus mainly on short-term effects. Future work should involve large-scale model tests and investigate the long-term strength changes of EICP-reinforced sand under different environmental conditions.

Author Contributions: Methodology, J.W.; Validation, X.L.; Formal analysis, L.P. and X.L.; Resources, J.W.; Data curation, J.Z., S.L. and X.D.; Writing—original draft, X.L.; Writing—review and editing, J.W.; Visualization, X.L.; Supervision, L.P.; Funding acquisition, J.W. All authors have read and agreed to the published version of the manuscript.

Funding: This research was funded by National Natural Science Foundation of China, grant number 42202309, 42172299 and Beijing Municipal Association for Science and Technology Golden Bridge Project Seed Project.

Institutional Review Board Statement: Not applicable.

Informed Consent Statement: Not applicable.

Data Availability Statement: The data presented in this study are available on request from the corresponding author. The data are not publicly available due to privacy.

Conflicts of Interest: We declare that none of the work contained in this manuscript is published in any language or currently under consideration at any other journal, and there are no conflicts of interest to declare. All authors have contributed to, read, and approved this submitted manuscript in its current form.

References

1. Debeleac, C.N.; Buraga, A.; Nastac, S.M. Experimental and Numerical Study in Dynamic Compaction of Weakly-Cohesive Soils. *Appl. Sci.* **2024**, *14*, 10129. [CrossRef]
2. Qian, Z.; Xiao, H.; Zhang, Z.; Nadakatti, M.M.; Chi, Y.; Wei, S. The Influence of Operation Times of Manual Tamping Device on Ballast Bed State. *Constr. Build. Mater.* **2024**, *414*, 135020. [CrossRef]
3. Fraccica, A.; Spagnoli, G.; Romero, E.; Arroyo, M.; Gómez, R. Permeation Grouting of Silt-Sand Mixtures. *Transp. Geotech.* **2022**, *35*, 100800. [CrossRef]
4. Li, Z.; Liu, J.; Xu, R.; Liu, H.; Shi, W. Study of Grouting Effectiveness Based on Shear Strength Evaluation with Experimental and Numerical Approaches. *Acta Geotech.* **2021**, *16*, 3991–4005. [CrossRef]
5. DeJong, J.T.; Mortensen, B.M.; Martinez, B.C.; Nelson, D.C. Bio-Mediated Soil Improvement. *Ecol. Eng.* **2010**, *36*, 197–210. [CrossRef]
6. Soon, N.W.; Lee, L.M.; Khun, T.C.; Ling, H.S. Factors Affecting Improvement in Engineering Properties of Residual Soil through Microbial-Induced Calcite Precipitation. *J. Geotech. Geoenviron. Eng.* **2014**, *140*, 04014006. [CrossRef]
7. Lv, C.; Li, W.-Q.; Tang, C.-S.; Zhu, C.; Pan, X.-H.; Zhang, X.; Shi, B. Characterization and Quantification of Calcite Distribution in MICP-Treated Sand Using μ-XRF Image Processing Technique. *Acta Geotech.* **2024**, *19*, 115–129. [CrossRef]
8. Bian, Y.; Chen, Y.; Zhan, L.; Ke, H.; Gao, Y.; Wang, Q.; Qi, G. An Enzyme-Induced Carbonate Precipitation Method for Zn^{2+}, Ni^{2+}, and Cr(VI) Remediation: An Experimental and Simulation Study. *Appl. Sci.* **2024**, *14*, 6559. [CrossRef]
9. Liu, K.-W.; Jiang, N.-J.; Qin, J.-D.; Wang, Y.-J.; Tang, C.-S.; Han, X.-L. An Experimental Study of Mitigating Coastal Sand Dune Erosion by Microbial- and Enzymatic-Induced Carbonate Precipitation. *Acta Geotech.* **2021**, *16*, 467–480. [CrossRef]
10. He, J.; Huang, A.; Ji, J.; Qu, S.; Hang, L. Enzyme Induced Carbonate Precipitation with Fibers for the Improvement of Clay Soil Slopes against Rainfall and Surface Runoff Erosions. *Transp. Geotech.* **2023**, *42*, 101074. [CrossRef]

11. Khoshdel Sangdeh, M.; Salimi, M.; Hakimi Khansar, H.; Dokaneh, M.; Zanganeh Ranjbar, P.; Payan, M.; Arabani, M. Predicting the Precipitated Calcium Carbonate and Unconfined Compressive Strength of Bio-Mediated Sands through Robust Hybrid Optimization Algorithms. *Transp. Geotech.* **2024**, *46*, 101235. [CrossRef]
12. Hamed Khodadadi, T.; Kavazanjian, E.; van Paassen, L.; DeJong, J. Bio-Grout Materials: A Review. *Grouting* **2017**, 1–12. [CrossRef]
13. Almajed, A.; Khodadadi Tirkolaei, H.; Kavazanjian, E. Baseline Investigation on Enzyme-Induced Calcium Carbonate Precipitation. *J. Geotech. Geoenviron. Eng.* **2018**, *144*, 04018081. [CrossRef]
14. Mortensen, B.M.; DeJong, J.T. Strength and Stiffness of MICP Treated Sand Subjected to Various Stress Paths. In *Proceedings of the Geo-Frontiers Congress 2011, Dallas, TX, USA, 13 March 2011*; ASCE Press: Reston, VA, USA, 2012; Volume 1, pp. 4012–4020.
15. Wang, J.; Mitrani, H.; Wipat, A.; Moreland, P.; Haystead, J.; Zhang, M.; Robertson, M.D. A Numerical Bio-Geotechnical Model of Pressure-Responsive Microbially Induced Calcium Carbonate Precipitation. *Appl. Sci.* **2024**, *14*, 2854. [CrossRef]
16. Lin, H.; Suleiman, M.T.; Brown, D.G. Investigation of Pore-Scale $CaCO_3$ Distributions and Their Effects on Stiffness and Permeability of Sands Treated by Microbially Induced Carbonate Precipitation (MICP). *Soils Found.* **2020**, *60*, 944–961. [CrossRef]
17. Chen, Y.; Han, Y.; Zhang, X.; Sarajpoor, S.; Zhang, S.; Yao, X. Experimental Study on Permeability and Strength Characteristics of MICP-Treated Calcareous Sand. *Biogeotechnics* **2023**, *1*, 100034. [CrossRef]
18. Gao, K.; Bick, P.; Suleiman, M.T.; Li, X.; Helm, J.; Brown, D.G.; Zouari, N. Wind Erosion Mitigation Using Microbial-Induced Carbonate Precipitation. *J. Geotech. Geoenviron. Eng.* **2023**, *149*, 04023053. [CrossRef]
19. Hemayati, M.; Nikooee, E.; Habibagahi, G.; Niazi, A.; Afzali, S.F. New Non-Ureolytic Heterotrophic Microbial Induced Carbonate Precipitation for Suppression of Sand Dune Wind Erosion. *Sci. Rep.* **2023**, *13*, 5845. [CrossRef]
20. Krishnan, V.; Khodadadi Tirkolaei, H.; Martin, K.; Hamdan, N.; van Paassen, L.A.; Kavazanjian, E. Variability in the Unconfined Compressive Strength of EICP-Treated "Standard" Sand. *J. Geotech. Geoenviron. Eng.* **2021**, *147*, 06021001. [CrossRef]
21. Venda Oliveira, P.J.; Rosa, J.A.O. Confined and Unconfined Behavior of a Silty Sand Improved by the Enzymatic Biocementation Method. *Transp. Geotech.* **2020**, *24*, 100400. [CrossRef]
22. Zhang, J.; Yin, Y.; Shi, W.; Bian, H.; Shi, L.; Wu, L.; Han, Z.; Zheng, J.; He, X. Strength and Uniformity of EICP-Treated Sand under Multi-Factor Coupling Effects. *Biogeotechnics* **2023**, *1*, 100007. [CrossRef]
23. Almajed, A.; Abbas, H.; Arab, M.; Alsabhan, A.; Hamid, W.; Al-Salloum, Y. Enzyme-Induced Carbonate Precipitation (EICP)-Based Methods for Ecofriendly Stabilization of Different Types of Natural Sands. *J. Clean. Prod.* **2020**, *274*, 122627. [CrossRef]
24. Cui, M.-J.; Lai, H.-J.; Hoang, T.; Chu, J. One-Phase-Low-pH Enzyme Induced Carbonate Precipitation (EICP) Method for Soil Improvement. *Acta Geotech.* **2021**, *16*, 481–489. [CrossRef]
25. Martin, K.; Tirkolaei, H.K.; Kavazanjian, E. Enhancing the Strength of Granular Material with a Modified Enzyme-Induced Carbonate Precipitation (EICP) Treatment Solution. *Constr. Build. Mater.* **2021**, *271*, 121529. [CrossRef]
26. *ASTM D2487-11*; ASTM Committee D-18 on Soil and Rock. Standard Practice for Classification of Soils for Engineering Purposes (Unified Soil Classification System). ASTM International: West Conshohocken, PA, USA, 2017.
27. Khodadadi Tirkolaei, H.; Javadi, N.; Krishnan, V.; Hamdan, N.; Kavazanjian, E. Crude Urease Extract for Biocementation. *J. Mater. Civ. Eng.* **2020**, *32*, 04020374. [CrossRef]
28. Zhao, Y.; Xiao, Z.; Fan, C.; Shen, W.; Wang, Q.; Liu, P. Comparative Mechanical Behaviors of Four Fiber-Reinforced Sand Cemented by Microbially Induced Carbonate Precipitation. *Bull. Eng. Geol. Environ.* **2020**, *79*, 3075–3086. [CrossRef]
29. Chaiyaput, S.; Arwaedo, N.; Kingnoi, N.; Nghia-Nguyen, T.; Ayawanna, J. Effect of Curing Conditions on the Strength of Soil Cement. *Case Stud. Constr. Mater.* **2022**, *16*, e01082. [CrossRef]
30. Decky, M.; Papanova, Z.; Juhas, M.; Kudelcikova, M. Evaluation of the Effect of Average Annual Temperatures in Slovakia between 1971 and 2020 on Stresses in Rigid Pavements. *Land* **2022**, *11*, 764. [CrossRef]
31. Alotaibi, E.; Arab, M.G.; Abdallah, M.; Nassif, N.; Omar, M. Life Cycle Assessment of Biocemented Sands Using Enzyme Induced Carbonate Precipitation (EICP) for Soil Stabilization Applications. *Sci. Rep.* **2022**, *12*, 6032. [CrossRef]
32. Falconer, K. *Fractal Geometry: Mathematical Foundations and Applications*; John Wiley & Sons: Hoboken, NJ, USA, 2004.
33. Lu, S.; Tang, H.; Zhang, Y.; Gong, W.; Wang, L. Effects of the Particle-Size Distribution on the Micro and Macro Behavior of Soils: Fractal Dimension as an Indicator of the Spatial Variability of a Slip Zone in a Landslide. *Bull. Eng. Geol. Environ.* **2018**, *77*, 665–677. [CrossRef]

Disclaimer/Publisher's Note: The statements, opinions and data contained in all publications are solely those of the individual author(s) and contributor(s) and not of MDPI and/or the editor(s). MDPI and/or the editor(s) disclaim responsibility for any injury to people or property resulting from any ideas, methods, instructions or products referred to in the content.